

1 Article

2 Characterization of S-band Dual-polarized Radar 3 Data for the Convective Rain Melting Layer 4 Detection in A Tropical Region

5 Feng Yuan ^{1, *}, Yee Hui Lee ², Yu Song Meng ³ and Jin Teong Ong ⁴

6 ¹ Temasek Laboratories, Nanyang Technological University, 50 Nanyang Avenue, Singapore 639798;
7 yuan0053@e.ntu.edu.sg

8 ² School of Electrical and Electronic Engineering, Nanyang Technological University, 50 Nanyang Avenue,
9 Singapore 639798; eyhlee@ntu.edu.sg

10 ³ National Metrology Centre, Agency for Science, Technology and Research (A*STAR), 1 Science Park Drive,
11 Singapore 118221; ysmeng@ieee.org, meng_yusong@nmc.a-star.edu.sg

12 ⁴ C2N Pte. Ltd., Singapore 199098

13 * Correspondence: yuan0053@e.ntu.edu.sg

14 Received: 02 October 2018

15 **Abstract:** In the tropical region, convective rain is a dominant rain event. However, very little
16 information is known about the convective rain melting layer. In this paper, S-band dual-polarized
17 radar data is studied in order to identify both the stratiform and convective rain melting layers in
18 the tropical region, with a focus on the convective events. **By studying and analyzing the above-**
19 **mentioned two types of rain events, amongst three radar measurements of reflectivity (Z),**
20 **differential reflectivity (Z_{DR}), and cross correlation coefficient (ρ_{HV}), the latter one is the best**
21 **indicator for convective rain melting layer detection. From two years (2014 and 2015) of radar and**
22 **radiosonde observations, 13 convective rain melting layers are identified with available 0°C**
23 **isothermal heights which are derived from radiosonde vertical profiles. By comparing the melting**
24 **layer top heights with the corresponding 0°C isothermal heights, it is found that for convective rain**
25 **events, the threshold to detect melting layer should be modified to $\rho_{HV} = 0.95$ for the tropical**
26 **region. The melting layer top and bottom heights are then estimated using the proposed threshold,**
27 **and it is observed from this study that the thickness of convective rain melting layer is around 2**
28 **times that of stratiform rain melting layer which is detected by using the conventional $\rho_{HV} = 0.97$.**

29 **Keywords:** melting layer; convective rain; dual-polarized radar; radiosonde

30

31 1. Introduction

32 The melting layer is the region where the ice crystals melt and transit into raindrop precipitation.
33 Therefore, it is also defined as the effective rain height. At this melting region, the reflectivity
34 increases and causes a bright band effect in radar measurements. Studying the characteristics of
35 melting layer is very important for accurate estimation of rainfall and microphysical characterization
36 of the cloud [1].

37 For satellite-to-earth communications and radar remote sensing applications, the melting layer
38 can cause both attenuation [2–5] and scattering [6–8] to the propagating signal at microwave
39 frequencies. It has been reported that the melting layer contributes significantly to the overall path
40 attenuation during the periods of stratiform rain for slant paths with low elevation angles [9].

41 Previously, reflectivity (Z) measurements from conventional radar have been used for
42 calculating the rainfall rate and detecting the melting layer bright band. However, the transition
43 between ice crystals and water droplets in melting layer cannot be well identified with only the
44 reflectivity measurements especially for convective rain events. Dual-polarized radar measurements

45 not only include the reflectivity, Z , measurement, but also the differential reflectivity, Z_{DR} , the linear
46 depolarization ratio, LDR, the specific differential propagation phase, K_{DP} , and the cross correlation
47 coefficient, ρ_{HV} [10]. Some of these parameters from dual-polarized radar measurement can provide
48 a better way to identify the melting layer. In a recent study of melting layer detection using dual-
49 polarized radar measurements, Giangrande et al. [1] proposed the use of three of these parameters
50 (Z , Z_{DR} , ρ_{HV}) for the detection of stratiform rain melting layer.

51 However, most of the existing studies [11, 12] on melting layer are for stratiform rain events, and
52 very limited research work was performed for convective rain events. This might be because
53 typically, there is no bright band effect in Z for convective rain events and therefore, it is very
54 difficult to identify the convective rain melting layer by using a single parameter from conventional
55 radar reflectivity measurements [13, 14].

56 Recently, Teshiba et al. [15] reported polarimetric melting signatures in a convective rainfall area
57 in central Oklahoma. They found that in one convective downdraft event, larger Z was observed at
58 lower altitude of below 3 km, and the downdraft resulted in a depression of melting layer height as
59 indicated by the vertical profiles of Z_{DR} and ρ_{HV} . In [16, 17], Shusse et al. presented the convective
60 rain melting layer characteristics in East China Sea region by using C-band polarimetric radar data.
61 After applying the classification method to separate the convective rain and stratiform rain on a 3-
62 hour event, they found that the melting layer in the convective region showed a marked decrease in
63 ρ_{HV} together with an increase in Z_{DR} around the 0°C isothermal height. They also concluded that the
64 average height of the melting layer signature maximum (defined by the level of the ρ_{HV} minimum
65 in the melting level) in the convective region is 0.46 km higher than that in the stratiform region.

66 In the tropical country of Singapore, there are frequent convective precipitations relative to the
67 temperate region. Therefore, it is ideal to study the convective rain melting layer in a tropical country
68 like Singapore. With the recent implementation of S-band dual-polarized radar in Singapore, both
69 the stratiform and convective melting layers will be investigated in details in this paper, with a focus
70 on the convective melting layer. By analyzing the recorded convective rain events, a method to detect
71 the convective rain melting layer will be proposed.

72 In the following, Section II provides a description of two meteorological databases (dual-
73 polarized radar data and radiosonde vertical profiles), which are used to detect the melting layer
74 structure and the corresponding 0°C isothermal heights. Section III presents the different
75 characteristics of stratiform and convective rain melting layer. An improved method to separate these
76 two types of rain cells are also proposed and discussed. In section IV, by studying and analyzing the
77 characteristics of convective rain melting layer based on recorded events, a method to detect
78 convective rain melting layer structure (top, bottom and thickness) based on a single value of ρ_{HV}
79 will be proposed and the performance of this threshold will be also discussed. Finally, conclusions
80 are presented in Section V.

81 2. Data Description

82 Two types of meteorological data sets are used for detecting the melting layers. S-band dual-
83 polarized radar data are used to detect the structure of melting layers including the top height,
84 bottom height and thickness. Radiosonde data providing the vertical profiles of temperature
85 information is used to find the 0°C isothermal height as the reference for the melting layer top
86 boundary [1].

87 2.1. Dual-polarized Weather Radar Data

88 In order to detect the melting layer, 2 years (2014 and 2015) data were collected from a dual-
89 polarized weather radar at Changi airport (1.35°N , 103.97°E) as shown in Figure 1. The total number
90 of radar scans collected from the year 2014 and 2015 is 93,891. The radar is operating in the S band at
91 a frequency of 2.71 GHz. It performs a full volume scan per 5 minutes with a maximum range of 120
92 km and a resolution of 250 m. For every interval of 5 minutes, the radar collects measurements at 8
93 elevation angles (1° , 1.5° , 3° , 5° , 7.5° , 10° , 20° , and 40°). The 5° elevation angle radar data is chosen for

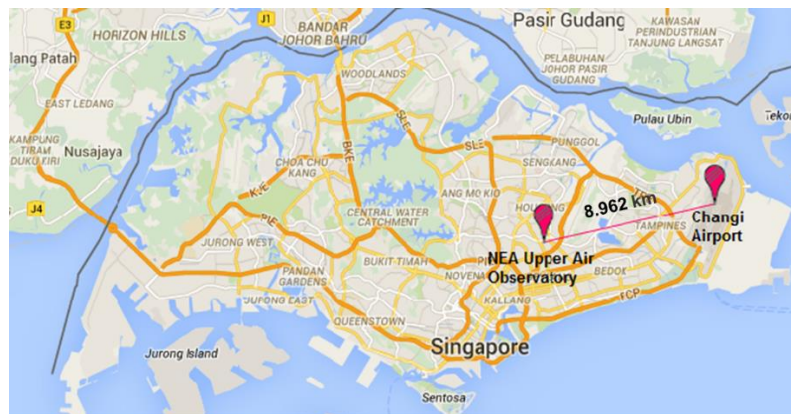
94 the detection and the analysis of the melting layer in this study. It was reported in [1, 17] that this
 95 elevation angle can provide relatively good vertical resolution/range and a good coverage range.

96 Dual-polarization radar can provide several types of measurements (reflectivity, differential
 97 reflectivity, cross-correlation coefficient, differential phase shift etc.), from the literature study [1],
 98 first three parameters were applied for stratiform rain melting layer detection. Therefore, these three
 99 parameters will be also studied and discussed in the following sections.

100 2.2. Radiosonde Data

101 Radiosonde data are acquired from an online database provided by the Department of
 102 Atmospheric Science, University of Wyoming [18].

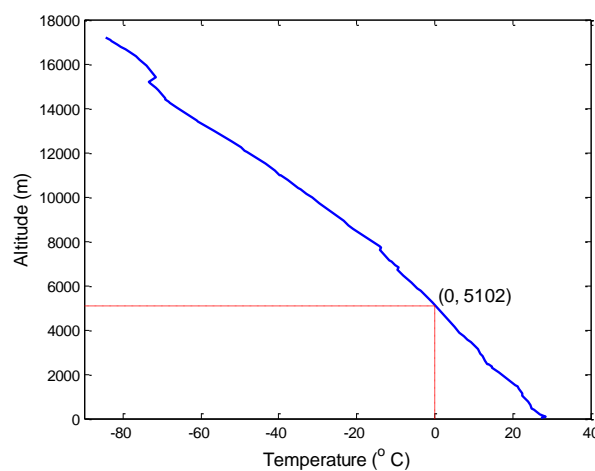
103 For the Singapore station, the raw experimental data are collected by the National Environment
 104 Agency (NEA) at Singapore upper air observatory (1.34°N, 103.89°E) as shown in Figure 1. The
 105 station number is 48698 in the World Meteorological Organization (WMO) network. The radiosonde
 106 observation times are twice per day at approximately 00:00 UTC and 10:00 UTC. The total number of
 107 radiosonde observations collected from the year 2014 and 2015 is 1,194.



108

109 **Figure 1.** Site locations of Changi airport and NEA upper air observatory.

110 The temperature and altitude information obtained from the radiosonde data can be used to
 111 estimate the 0°C isothermal height as shown in Figure 2. In order to determine the 0°C isothermal
 112 levels for the corresponding rain events, the radiosonde data collected in Year 2014 and 2015, are
 113 processed as a reference for the melting layer top heights [1, 19].



114

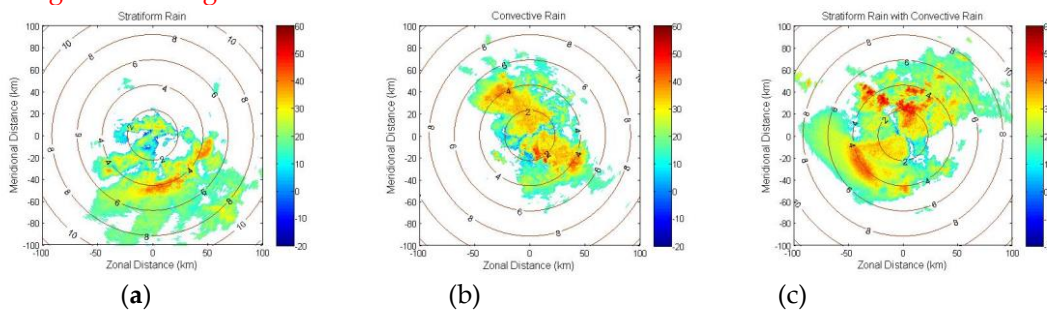
115 **Figure 2.** Radiosonde altitude and temperature measured at 10:00 UTC on 21st April 2014 with the
 116 indication of 0° C isothermal height.

117 3. Methodology

118 3.1. Identification of Melting Layer for Different Rain Cases

119 To investigate and identify the characteristics of melting layers in the tropical region, the dual-
 120 polarized radar data from three different categories of rains are processed and analyzed. The three
 121 different rain categories include stratiform rain only, convective rain only, and stratiform rain
 122 together with convective rain. For example, one radar PPI (Plan Position Indicator) image of the
 123 reflectivity measurement (Z) taken from 05:45 UTC on 21st April 2014 at an elevation angle of 5° is
 124 shown in Figure 3 over a 200 km by 200 km square area.

125 As shown in Figure 3, the center is Changi airport where the dual-polarized radar is located.
 126 Since the height information is very important for melting layer detection, the contour lines indicating
 127 the heights above ground level (a.g.l.) of the pixels are included in the figures. The contour lines at 2
 128 km intervals are specified as shown in Figure 3. For the 5° elevation angle, the maximum height is
 129 8.72 km a.g.l. at the range of 100 km.



130
131

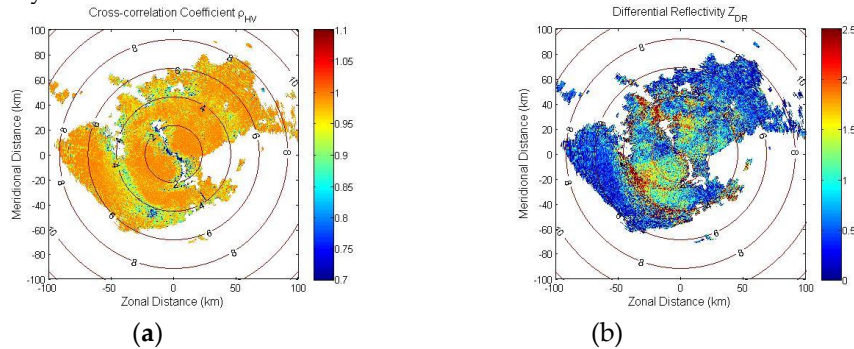
132 **Figure 3.** Dual-polarized radar PPI images of Z for (a) stratiform rain only, (b) convective rain,
 133 and (c) stratiform rain together with convective rain.

134 In Figure 3(a), **maximum reflectivity** is observed at a height of around 4 km a.g.l., which are due
 135 to the bright band effect of stratiform rain melting layer. Similar effect can be also observed in Figure
 136 3(c) in the south western part at a similar height of around 4 km a.g.l.. For convective rain event
 137 shown in Figure 3(b), **there is no any clear bright band effect since the maximum reflectivity** spreads
 138 over the height ranging from ground level to around 5 km a.g.l.. In this rain region, the maximum
 139 reflectivity is recorded to be 56 dBZ, **which is equivalent to a rainfall rate of 169 mm/hr** [20]. This high
 140 rainfall rate clearly is categorized as convective rain as reported in [21]. Similar convective rain cell
 141 can also be observed in Figure 3(c) in the northern part. The maximum reflectivity in the northern
 142 part of Figure 3(c) is at 57.5 dBZ (**i.e., rainfall rate of 217 mm/hr**) which clearly indicates a convective
 143 rain event. Therefore, it is clear from Figure 3(a) and (c) that for the stratiform rain, **maximum**
 144 **reflectivity** is concentrated in the melting layer area with similar altitude, the bright band, while for
 145 the convective rain the **maximum reflectivity** spreads across a vertical range from ground level to 5
 146 km a.g.l. and therefore, the melting layer cannot be easily identified.

147 To detect the melting layer accurately, as reported in the Giangrande model [1], three
 148 measurements (Z, Z_{DR}, ρ_{HV}) from the dual-polarized radar should be processed and analyzed.
 149 **Giangrande et al. proposed to use these three parameters for the detection of stratiform rain melting**
 150 **layer. It suggested that the value of ρ_{HV} should fall between 0.90 and 0.97, the maximum value of**
 151 **Z_{DR} should be within the interval of 0.8 to 2.5 dB and the maximum value of Z should fall between**
 152 **30 and 47 dBZ. All these three criteria should be fulfilled in the same window of 500 m for a melting**
 153 **layer to be identified.**

154 Taking the stratiform rain together with convective rain case in Figure 3(c) as an example, radar
 155 PPI images of ρ_{HV} and Z_{DR} at the same moment are plotted in Figure 4. In Figure 4(a), a light circle
 156 ring with ρ_{HV} around 0.95 can be observed at the height around 4 km a.g.l. indicating the melting
 157 layer. The height of convective rain melting layer in the northern part is found to be slightly higher
 158 between 4 km a.g.l. to 5 km a.g.l. as compared to the stratiform rain melting layer in the south western
 159 part. In Figure 4(b) for stratiform rain region, the maximum value of differential reflectivity Z_{DR} can
 160 be found around the melting layer area region, however for the convective rain region, it is scattered.
 161 Similar patterns are also observed for all other rain events processed. Therefore, among these three

162 measurements (Z, Z_{DR}, ρ_{HV}), it can be concluded that ρ_{HV} is the best indicator for melting layer
 163 detection, since it has the ability to detect both the stratiform and convective rain melting layers. In
 164 the next section, differentiation of the two types of stratiform and convective rain melting layers will
 165 be carried out. By processing three parameters (Z, Z_{DR}, ρ_{HV}) of radar measurements along the slant
 166 path from each type of rain events, the characteristics of stratiform and convective rain melting layers
 167 will be analyzed and discussed.



168
169

170 **Figure 4.** Dual-polarized radar PPI images of (a) ρ_{HV} , and (b) Z_{DR} at 05:45 UTC on 21st April 2014
 171 with an elevation angle of 5° .

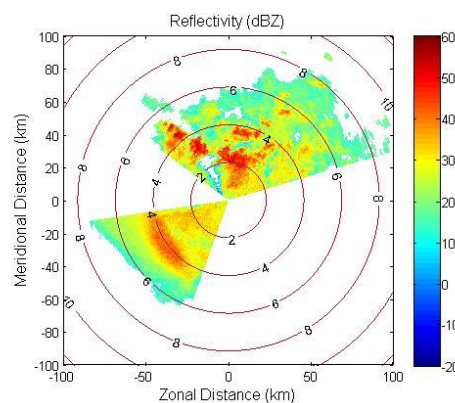
172 3.2. Differentiation between Stratiform and Convective Rain

173 In order to better understand the characteristics of stratiform rain and convective rain cells, a
 174 method to differentiate these two types of rain is proposed in this section. By considering the top
 175 height of the melting layer to be at the 0°C isothermal height and the thickness is around 500 m [1,
 176 22, 23], it is noted that in the tropical region, the height of stratiform rain melting layer is typically
 177 within 3 km a.g.l. to 5 km a.g.l. [12, 24].

178 The proposed method for the classification of the stratiform rain cell and convective rain cell in
 179 this study is given as such:

- 180 1. a reflectivity of 30 dBZ [1] is taken as the threshold for melting layer detection, if the maximum
 181 reflectivity is above or equal to the threshold within the height range of 3 km a.g.l. to 5 km a.g.l.,
 182 then this ray is considered to be passing through the stratiform rain cell.
- 183 2. with the same threshold of 30 dBZ, if the maximum reflectivity is above or equal to the threshold
 184 within the height range of 1 km a.g.l. to 3 km a.g.l., then this ray is considered to be passing
 185 through the convective rain cell.

186 After classifying all the slant rays, a clear separation of the stratiform rain cell in southwest and
 187 the convective rain cell in north from Figure 3(c) is plotted in Figure 5. It can be observed that the
 188 bright band area from stratiform rain melting layer is clear in the south western region of the plot.
 189 Although the convective rain cell can be identified in the northern region of the plot, there is no clear
 190 indication of the melting layer for the convective rain cell.

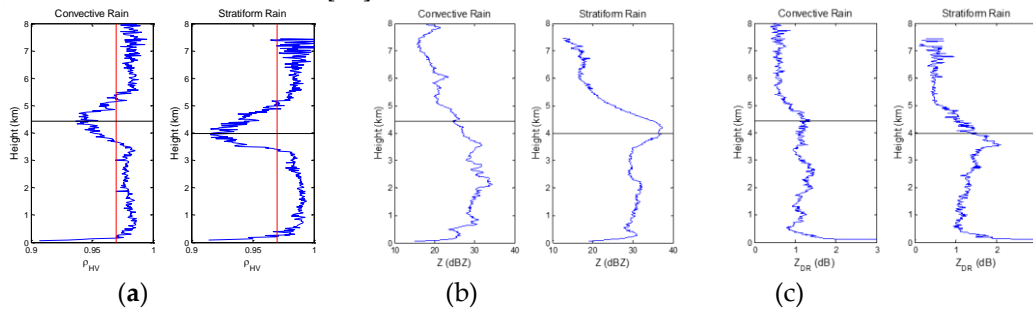


191

192 **Figure 5.** Radar reflectivity PPI for two separated rain events at 05:45 UTC on 21st April 2014.

193 Therefore, in order to identify the convective melting layer and better understand the stratiform
 194 melting layer, vertical profiles of ρ_{HV} , Z and Z_{DR} for the two categories of rain cells are combined
 195 and averaged across the same height along each slant ray. The averaged vertical profiles of 3 radar
 196 parameters for the convective rain cell and the stratiform rain cell are presented in Figure 6. For the
 197 stratiform rain cell, 118 slant path profiles are used for averaging and for the convective rain cell, 61
 198 slant path profiles are averaged. The vertical red line in Figure 6(a) is a reference line representing
 199 $\rho_{HV} = 0.97$ [1]. The lower and upper boundary of the melting layer can be identified from the
 200 interception point between the measured ρ_{HV} and the red line. The horizontal black line in Figure
 201 6(a) indicates the minimum point of the measured ρ_{HV} within the melting layer. From Figure 6, it
 202 can easily be seen that for the stratiform rain event, as indicated by the Giangrande model, the
 203 maximum value of Z and Z_{DR} in Figure 6(b) and (c) respectively corresponds well to the minimum
 204 value of ρ_{HV} in Figure 6(a) by the black line in all plots. This occurs roughly around the same height
 205 of 4 km a.g.l..

206 However, for the convective rain event, there is no obvious maximum in the Z and Z_{DR} values
 207 in Figure 6(b) and Figure 6(c) respectively. Two local maximums can be observed around the height
 208 of 2.5 km a.g.l.. However, this is not the melting layer height for a convective rain cell in the tropical
 209 region. In [24], the 0°C isothermal heights for tropical region are reported to be typically within the
 210 range of [4.2 km, 5.5 km]. It is reported in [1, 19, 25] that the 0°C isothermal height is generally taken
 211 as the top boundary of melting layers. Examining the value of ρ_{HV} along the slant path of the
 212 convective rain cell in Figure 6(a), by using a threshold of $\rho_{HV} < 0.97$, the melting layer height of the
 213 convective rain cell can be detected. In addition, it can be observed that the ρ_{HV} minimum level of
 214 melting layer in the convective rain region is around 0.5 km higher than that of the stratiform rain
 215 region, which is also discussed in [17].



216
217

218 **Figure 6.** Averaged vertical profiles of (a) ρ_{HV} , (b) Z and (c) Z_{DR} at the same height for convective
 219 rain cell and stratiform rain cell at 05:45 UTC on 21st April 2014.

220 Therefore, the results show that the cross-correlation coefficient ρ_{HV} can indicate the melting
 221 layer height not only for stratiform rain cells but also for convective rain cells. The variation and the
 222 maximum value of Z and Z_{DR} are not so useful for convective rain cell melting layer detection.

223 3.3. Proposed Threshold for Convective Rain Melting Layer Detection

224 After processing two-year dual-polarized radar data by using the differentiation and
 225 categorization methods as discussed above, 13 convective rain events with corresponding melting
 226 layers found via the radiosonde temperature profiles in the years 2014 and 2015. These events are
 227 listed in Table 1 with their corresponding date and time information. Since the top boundary of the
 228 melting layer is typically located where the 0°C isothermal height is [1, 19, 25], the vertical profiles of
 229 temperature data measured by the radiosonde are processed in order to retrieve the 0°C isothermal
 230 height. In Table 1, the convective rain with melting layers detected are found to have the
 231 corresponding radiosonde measurements (at 00:00 UTC and 10:00 UTC) of 0°C isothermal height
 232 within 6 hours. The time difference for these events can be as small as 1 hour to as large as 5 hours
 233 and 40 minutes. Due to the limitation in radiosonde data resolution, linear interpolation technique is
 234 applied to the temperature and height data. From Table 1, it can be observed that for these recorded
 235 events, the range of 0°C isothermal height is from around 4500 m to 5100 m with very small variations

236 throughout the whole year. This is because Singapore is in the equatorial region where seasonal
 237 temperature fluctuation is very small compared to the subtropical and temperate regions.
 238

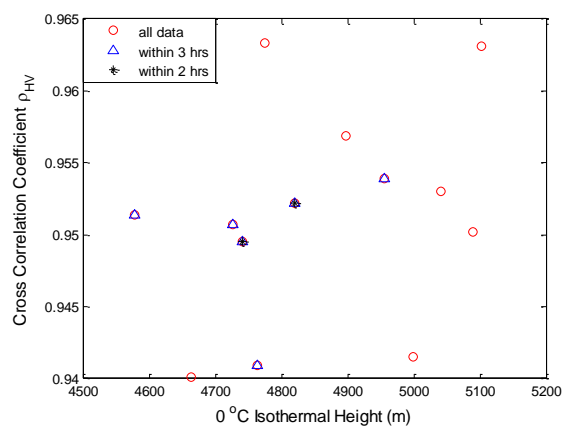
Table 1. Convective rain melting layer events with closest radiosonde data.

Event	Time (UTC)	Time Difference comparing with Radiosonde	0°C Isothermal Height (m)	Height of Maximum Reflectivity
04 Jan 2014	18:40	5hr 20min	4775	2092
05 Jan 2014	20:25	3hr 35min	4663	675
21 Apr 2014	05:45	4hr 15min	5102	2135
05 Jun 2014	06:15	3hr 45min	4898	1133
14 Jun 2014	05:50	4hr 10 min	5090	1961
30 Nov 2014	23:00	1hr	4820	2593
04 Dec 2014	01:25	1hr 25min	4741	1830
12 Aug 2015	02:20	2hr 20min	4764	2462
01 Oct 2015	21:40	2hr 20min	4578	174
27 Oct 2015	21:00	3hr	4727	1155
08 Dec 2015	18:20	5hr 40min	5041	218
12 Dec 2015	14:10	4hr 10min	4999	1133
13 Dec 2015	07:45	2hr 15min	4955	2114

239

240 In order to determine the threshold value of ρ_{HV} for the detection of the top boundary of the
 241 convective rain cell melting layer and ensure that this detected top boundary corresponds to the 0°C
 242 isothermal height obtained from the radiosonde data, the 0°C isothermal height with its
 243 corresponding ρ_{HV} for each convective rain cell is plotted in Figure 7. Among the recorded events,
 244 the time difference between the recorded dual-polarized radar data and the closest radiosonde data
 245 are divided into 3 categories: 2 convective rain cells are detected within 2 hours of the radiosonde, 6
 246 convective rain cells are detected within 3 hours and all the events are within 6 hours as listed in
 247 Table 1.

248 From Figure 7, the ρ_{HV} values at 0°C isothermal heights for all the 13 events fall into the range
 249 of 0.94 to 0.965, which are all less than the threshold of 0.97 proposed in the Giangrande model [1].
 250 Therefore, for the convective rain cell melting layer detection, the threshold of 0.97 is too high and
 251 can cause overestimation. From the analysis of results shown in Figure 7, data with less time
 252 difference is found to be more concentrated together due to the relatively small drifting effect. In
 253 order to propose an appropriate ρ_{HV} value for convective rain cell melting layer detection, we focus
 254 on the data with 0°C isothermal height that is less than 3 hours apart. It can be observed that most of
 255 ρ_{HV} values are around 0.95 in Figure 7.



256

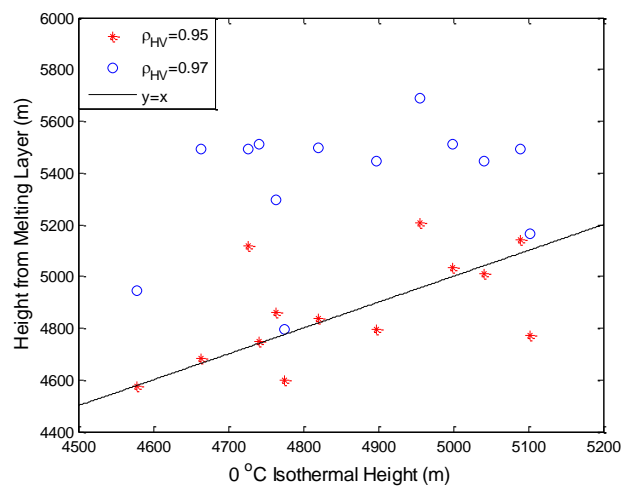
257 **Figure 7.** Scatter plot between the 0°C isothermal height and the corresponding ρ_{HV} value for
 258 convective rain melting layer.

259 Therefore, the proposed criterion for convective rain cell melting layer detection in this study is
 260 given as: For convective rain cell, if the measured cross correlation coefficient ρ_{HV} is smaller than
 261 0.95, this level is treated to be in the melting layer.

262 4. Results and Discussion

263 4.1. Performance Evaluation of Proposed Threshold

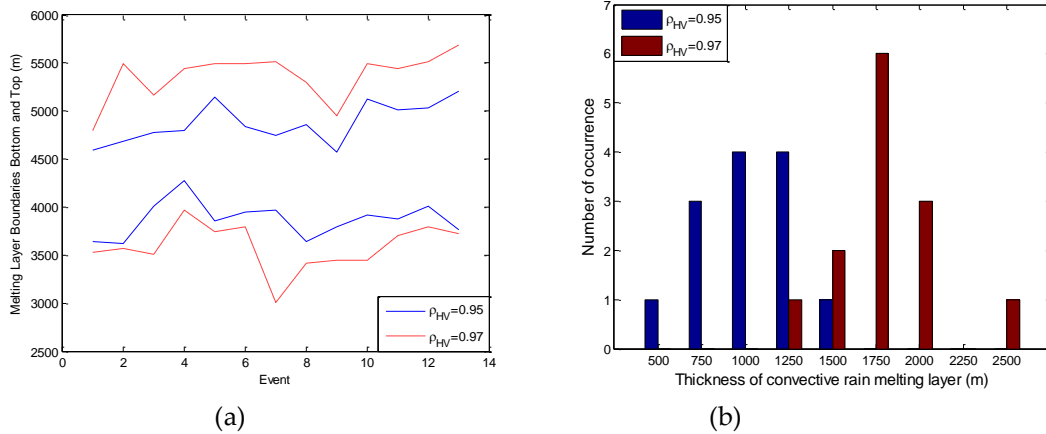
264 In order to evaluate the performance of the proposed threshold for detecting the top boundary of
 265 the convective rain melting layer, a scatter plot between the 0°C isothermal height and the top
 266 boundary of the melting layer detected by the new proposed threshold and by the Giangrande model
 267 [1] are both plotted in Figure 8. The black line is $y = x$, which represents when the height of the
 268 melting layer top boundary is equal to the 0°C isothermal height. From Figure 8, the top boundary of
 269 the melting layer detected by using the new proposed threshold ($\rho_{HV} = 0.95$) are observed much
 270 closer to the 0°C isothermal heights, and the threshold ($\rho_{HV} = 0.97$) from the Giangrande model
 271 tends to overestimate the convective melting layer top heights.



272

273 **Figure 8.** Scatter plot between 0°C isothermal height and convective rain melting layer top height detected using
 274 two different thresholds.

275 By applying the new proposed threshold ($\rho_{HV} = 0.95$), the melting layer top and bottom heights
 276 are estimated for each convective rain cell as shown in Figure 9(a). By taking the difference between
 277 the melting layer top height and bottom height, the thickness of the convective rain cell melting layer
 278 can be determined. The histograms of convective rain melting layer thickness by using the two
 279 different thresholds (proposed threshold of 0.95 and Giangrande threshold of 0.97) are plotted in
 280 Figure 9(b) with the bin size of 250 m. It can be observed that for the convective rain melting layer
 281 thickness detected by the proposed threshold ($\rho_{HV} = 0.95$), the minimum thickness is around 500 m,
 282 and the maximum is around 1500 m with most of the thickness around 1000m. While for the
 283 convective rain melting layer thickness detected by using the Giangrande threshold ($\rho_{HV} = 0.95$),
 284 the minimum thickness is around 1250 m, and maximum is around 2500 m with most of the thickness
 285 around 1750 m. As discussed in the previous section, the threshold from the Giangrande model tends
 286 to overestimate the convective melting layer top heights, therefore it also overestimates the thickness
 287 of the convective rain melting layer.



288
289
290
291

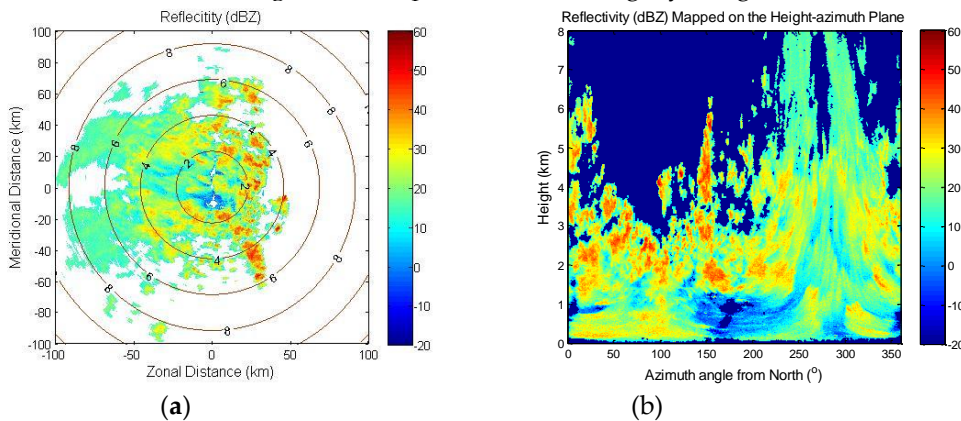
Figure 9. (a) Melting layer bottom and top heights of convective rain cell (b) Histogram of convective rain cell melting layer thickness using two different thresholds.

292 As reported in [17], the convective rain melting layer thickness is about 1.5 to 2 times that of the
293 stratiform rain melting layer. The stratiform rain melting layer thickness is found to be around 500 m
294 [1, 22, 25]. Therefore, the convective rain cell melting layer is around 750 to 1000 m. Using the
295 Giangrande model, the thickness of convective rain melting layer is around 3 to 4 times that of the
296 stratiform rain melting layer height as shown in Figure 9(b). Clearly, the model overestimates the
297 thickness of the convective rain melting layer. From our proposed model, the convective rain melting
298 layer is found to be approximately 2 times that of the stratiform rain melting layer (Figure 9), this
299 is consistent with those reported in [17]. Therefore, the new proposed threshold is more accurate for
300 detecting the convective rain melting layer thickness.

301 *4.2. Special Case for Convective Rain*

302 One special case with convective rain updraft effect recorded at 14:55 UTC on the 14th June 2014
303 as shown in Figure 10 was identified through processing the dual-polarized radar data. Figure 10 (a)
304 shows many simultaneous small-scale convective rain cells scattered over the eastern part. To study
305 the vertical structure of these small-scale convective rain cells, the radar reflectivity mapped on the
306 height-azimuth plane for Figure 10 (a) is plotted in Figure 10 (b). The maximum reflectivity of this
307 convective rain event is recorded at an azimuth angle of 150° with a maximum reflectivity of 52.5
308 dBZ (i.e., rainfall rate of 95 mm/hr). This represents a heavy convective rain event and the rain cell
309 height extends up to above 6 km *a.g.l.*. This height is around 1 km higher than the average 0°C
310 isothermal heights which is reported in [24] to be within [4.2 km, 5.5 km] (processed from one-year
311 radiosonde temperature vertical profiles in Singapore [24]). In [1, 19, 25], it was reported that the 0°C
312 isothermal height is close to the top boundary of the melting layer and the rain height. Therefore, the
313 raindrops around 6 km *a.g.l.* in this convective rain event is most probably due to the lifting effect
314 from an updraft phenomenon. For this type of convective rain events, the melting layer cannot clearly
315 be identified due to the mixing of raindrops with the melting layer region.

316
317



318 **Figure 10.** Radar reflectivity measured at 14:55 UTC on 14th June 2014 (a) PPI image (b) mapped on
319 the height–azimuth plane.

320 5. Conclusion

321 In this paper, S-band dual-polarized radar data are processed for the analysis of the melting
322 layer structure for both convective and stratiform rains in the tropical region, especially for the
323 convective rain. By investigating three radar measurements (ρ_{HV} , Z , Z_{DR}), the cross-correlation
324 coefficient ρ_{HV} is found to be the best indicator for the identification of the melting layer particularly
325 for convective rain cells.

326 By studying the heights of maximum reflectivity for stratiform rain cells and convective rain
327 cells, a method is proposed to differentiate and categorize stratiform rain cell and convective rain cell.
328 13 convective rain cells melting layers with associated radiosonde temperature profiles are found in
329 the year of 2014 and 2015. Taking 0°C isothermal height from radiosonde profile as the top boundary
330 for the melting layer, it is found that for convective rain events in the tropical region, the threshold
331 for melting layer detection shall be revised as $\rho_{HV} = 0.95$. By applying this newly proposed
332 threshold, the thickness of convective rain melting layer is found to be more accurate. The detected
333 melting layer thickness for convective rain is around 1000 m, which is around 2 times that of the
334 melting layer thickness of the stratiform rain.

335 In addition, a special case of convective rain cell is investigated. The maximum reflectivity of
336 this convective rain cell extends up to above 6 km due to the lifting effect. For this type of convective
337 rain events, the melting layer cannot clearly be identified due to the mixing of raindrops within the
338 melting layer region.

339 References

- 340 1. Giangrande, S. E.; Krause, J. M.; Ryzhkov, A. V. Automatic designation of the melting layer with a
341 polarimetric prototype of the WSR-88D radar. *J. Appl. Meteor.* 2007, 47, 1354-1364.
- 342 2. Zhang, W.; Karhu, S. I.; Salonen, E. T. Predictions of radiowave attenuations due to a melting layer of
343 precipitation. *IEEE Trans. Antennas Propag.* 1994, 42, 492-500.
- 344 3. Romo, J. A.; Maruri, M.; Pérez-Fontán, F.; Fernández, I. Characterization of maximum radar reflectivity
345 height during stratiform rain events. *IEEE Trans. Antennas Propag.* 2012, 60, 4884-4891.
- 346 4. Lerber, A.; Moisseev, D.; Leinonen, J.; Koistinen, J.; Hallikainen, M. T. Modeling Radar Attenuation by a
347 Low Melting Layer with Optimized Model Parameters at C-Band. *IEEE Trans. Geosci. Remote Sens.* 2015,
348 53, 724-737.
- 349 5. Pujol, O.; Mesnard, F.; Sauvageot, H. Effects of Melting Layer in Airborne Meteorological X-Band Radar
350 Observations. *IEEE Trans. Geosci. Remote Sens.* 2012, 50, 2318-2324.
- 351 6. Russchenberg, H. W. J.; Ligthart, L. P. Backscattering by and propagation through the melting layer of
352 precipitation: a new polarimetric model. *IEEE Trans. Geosci. Remote Sens.* 1996, 34, 3-14.
- 353 7. Raynaud, L.; Chenerie, I.; Lemorton, J. Modeling of radiowave scattering in the melting layer of
354 precipitation. *IEEE Trans. Geosci. Remote Sens.* 2000, 38, 1574-1584.
- 355 8. Marzano, F. S.; Bauer, P. Sensitivity analysis of airborne microwave retrieval of stratiform precipitation to
356 the melting layer parameterization. *IEEE Trans. Geosci. Remote Sens.* 2001, 39, 75-91.
- 357 9. Panagopoulos, A. D.; Arapoglou, P. M.; Cottis, P. G. Satellite communications at Ku, Ka, and V bands:
358 propagation impairments and mitigation techniques. *IEEE Commun. Surv. Tutor.* 2004, 6, 2-14.
- 359 10. Vivekanandan, J.; Zrnic, D. S.; Ellis, S. M.; Oye, R.; Ryzhkov, A. V.; Straka, J. Cloud microphysics retrieval
360 using S-band dual-polarization radar measurements. *Bull. Amer. Meteorol. Soc.* 1999, 80, 381-388.
- 361 11. Wilson, C. L.; Tan, J.; Goddard, J. W. F.; Ong, J. T. Radar vertical profiles and melting layer studies from an
362 S-band Doppler polarization-diversity radar Campaign in Singapore. 30th International Conference on
363 Radar Meteorology – American Meteorological Society 1998, 423-425.
- 364 12. Wilson, C. L.; Tan, J. Melting layer studies in Singapore: experimental results from an S-band doppler
365 polarisation-diversity radar. *Physics and Chemistry of the Earth, Part B: Hydrology, Oceans and
366 Atmosphere* 2000, 25, 1129-1132.

- 367 13. Kalogiros, J.; Anagnostou, M. N.; Anagnostou, E. N.; Montopoli, M.; Picciotti, E.; Marzano, F. S. Correction
368 of polarimetric radar reflectivity measurements and rainfall estimates for apparent vertical profile in
369 stratiform rain. *J. Appl. Meteor. Climatol.* 2013, 52, 1170–1186.
- 370 14. Matrosov, S. Y.; Kingsmill, D. E.; Martner, B. E.; Ralph, F. M. The utility of X-band polarimetric radar for
371 quantitative estimates of rainfall parameters. *J. Hydrometeor.* 2005, 6, 248–262.
- 372 15. Teshiba, M. S.; Chilson, P. B.; Ryzhkov, A. V. T.; Schuur, J.; Palmer, R. D. A combined wind profiler and
373 polarimetric weather radar method for the investigation of precipitation and vertical velocities. *J. Atmos.*
374 *Oceanic Technol.* 2008, 26, 1940–1955.
- 375 16. Shusse, Y.; Nakagawa, K.; Takahashi, N.; Satoh, S.; Iguchi, T. Characteristics of polarimetric radar variables
376 in three types of rainfalls in Baiu front event over the East China Sea. *J. Meteor. Soc. Japan* 2009, 87, 865–
377 875.
- 378 17. Shusse, Y.; Takahashi, N.; Nakagawa, K.; Satoh, S.; Iguchi, T. Polarimetric radar observation of the melting
379 layer in a convective rainfall system during the rainy season over the East China sea. *J. Appl. Meteor.*
380 *Climatol.* 2011, 50, 354–367.
- 381 18. Department of Atmospheric Science, University of Wyoming,
382 <http://weather.uwyo.edu/upperair/sounding.html>
- 383 19. Wolfensberger, D.; Scipion, D.; Berne, A. Detection and characterization of the melting layer based on
384 polarimetric radar scans. *Q. J. R. Meteorol. Soc.* 2015, 142, 108–124.
- 385 20. Alexander, V. R.; Scott, E. G.; Terry, J. S. Rainfall estimation with a polarimetric prototype of WSR-88D. *J.*
386 *Appl. Meteor.* 2004, 44, 502–515.
- 387 21. Capsoni, C.; Luini, L.; Paraboni, A.; Riva, C.; Martelluci, A. A new prediction model of rain attenuation that
388 separately accounts for stratiform and convective rain. *IEEE Trans. Antennas Propag.* 2009, 57, 196–203.
- 389 22. Fabry, F.; Zawadzki, I. Long-term radar observations of the melting layer of precipitation and their
390 interpretation. *J. Atmos. Sci.* 1995, 52, 838–851.
- 391 23. Hall, W.; Rico-Ramirez, M. A.; Kramer, S. Classification and correction of the bright band using an
392 operational C-band polarimetric radar. *Journal of Hydrology* 2015, 531, 248–258.
- 393 24. Yuan, F.; Manandhar, S.; Lee, Y. H.; Meng, Y. S. Model comparison for estimating cloud liquid water
394 content and attenuation in tropical region. *IEEE Region 10 Conference (TENCON) 2016*, 1317–1320.
- 395 25. ITU-R: Recommendation P.839-3. Rain height model for prediction methods. *Propagation in non-ionized*
396 *media* 2001.